Biomech Model Mechanobiol
DOI 10.1007/s10237-008-0137-y

ORIGINAL PAPER

# Probing the influence of myelin and glia on the tensile properties of the spinal cord

**David I. Shreiber · Hailing Hao · Ragi AI. Elias**

Received: 26 February 2008 / Accepted: 29 July 2008


**Abstract** Although glia have been historically classified as the structurally supporting cells of the central nervous system, their role in tissue mechanics is still largely unstudied. The influence of myelin and glia on the mechanical properties of spinal cord tissue was examined by testing embryonic day 18 chick embryo spinal cords in uniaxial tension following disruption of the glial matrix using either ethidium bromide (EB) or an antibody against galactocerebroside ($\alpha$GalC) in the presence of complement. Demyelination was confirmed by myelin basic protein immunoreactivity and quantified using osmium tetroxide staining. A substantial loss of astrocytes and oligodendrocytes concurrent with demyelination was observed following EB injection but not $\alpha$GalC injection. No morphological changes were observed following injection of saline or IgG with complement as controls for EB and $\alpha$GalC. Demyelinated spinal cords demonstrated significantly lower stiffness and ultimate tensile stress than myelinated spinal cords. No significant differences were observed in the tensile response between the two demyelinating protocols. The results demonstrate that the glial matrix provides significant mechanical support to the spinal cord, and suggests that myelin and cellular coupling of axons via the glial matrix in large part dictates the tensile response of the tissue.

**Keywords** Tissue mechanics · Axonal injury · Spinal cord injury · Myelin · Astrocyte · Oligodendrocyte

D. I. Shreiber (✉) · H. Hao · R. AI. Elias
Department of Biomedical Engineering, Rutgers,
The State University of New Jersey, 599 Taylor Road,
Piscataway, NJ 08854, USA
e-mail: shreiber@rci.rutgers.edu

## 1 Introduction

Glia, the primary non-neuronal cells of the central nervous system (CNS), were initially believed to bind or glue neurons together and/or provide a supporting scaffold for the neurons (Virchow 1856; Schultze 1866). Through decades of research, it is now recognized that glia provide specialized biological and regulatory functions that are essential to neurophysiology. Oligodendrocytes have long been known to produce myelin, the highly differentiated membrane structure that wraps around axons to enhance conduction velocity and induce saltatory conduction of neuropotentials. More recently, astrocytes have been recognized not only as just regulators of homeostasis and blood–brain barrier functions but also as excitable support cells that contribute to a myriad of functions, including synapse formation and function, adult neurogenesis, and cerebrovascular tone (see Volterra and Meldolesi 2005 for a recent review).

Nevertheless, unlike most other 'soft' tissue, CNS tissue does not maintain a significant, extracellular, connective tissue element, and the original postulate that glia support the network of interconnected neurons and their dendritic and axonal processes remains possible. The contribution of these "cellular scaffolds" (Schultze 1866) to the overall mechanical properties would strongly influence the tissue's tolerance to loading conditions experienced during trauma. Additionally, it is now known that the mechanical environment, including intrinsic stresses generated by cells contracting against a substrate and extrinsic stresses delivered to cells through that substrate, is an important regulator of function in many cell types, including neurons and glia (Heidemann and Buxbaum 1994; Flanagan et al. 2002; Georges et al. 2006). Several neuron types have demonstrated increased neurite branching and growth on or in compliant substrates (Balgude et al. 2001; Flanagan et al. 2002; Georges et al.

2006), which generally induces astrocyte quiescence. Conversely, astrocyte proliferation and migration are improved on stiffer substrates.

Stress- or stretch-sensitive behavior by constitutive cells is common in load-bearing tissues such as bone, tendons, and blood vessels, and these stresses and/or strains may similarly regulate phenotypic behavior of CNS cells. Alternatively, glia and neurons may act in concert to alter the physical structure of the tissue to guard against the influence of these extrinsic conditions in a 'form-follows-function' manner. Lu et al. (2006) recently showed that the stiffness of astrocytes in the hippocampus and of Müller cells (bipolar glia) in the retina was significantly lower than that of pyramidal neurons and bipolar and amacrine retinal neurons, which the glia support, respectively. It was suggested that glia do not rigidly support neurons as much as provide a soft, embedding material that provides sufficient compliance to respond to normal changes in intracranial pressure and to perhaps protect against abnormal forces experienced during trauma. Additionally, glia may regulate the mechanical properties of particular regions of CNS tissue, such as the hippocampus, to provide additional targeting information for synaptogenesis. The mechanical properties of the granule layers of the post-natal rat hippocampus present a gradient of mechanical properties (Elkin et al. 2007) that may evolve and correlate to targeting axons during tissue morphogenesis.

Moreover, some CNS tissues, particularly the spinal cord (although likely some cranial nerves as well), routinely experience physical stress during routine movements. For example, MR studies have shown that the human cervical spinal cord experiences 6–10% strain during flexion (Yuan et al. 1998). The spinal cord is a longitudinally organized structure that includes an H-shaped, gray matter interior within an exterior of ascending and descending tracts of white matter. The spinal cord is suspended by the dentate ligaments, which are extensions of the pia mater meningeal layer and connect to the arachnoid-lined dura mater. Dorsal and ventral roots exit the cord to carry afferent and efferent information. Blood is supplied from two posterior spinal arteries and one anterior spinal artery, from which branches emerge. Both routine and injurious levels of stress and strain are somehow distributed throughout these spinal cord tissues and the cells that comprise these substructures.

The physical microstructure of white matter represents an intriguing tissue form to study further and appreciate the role of glia, particularly oligodendrocytes, in tissue and cellular mechanics. White matter consists generally of bundles of axons aligned in parallel that are myelinated by oligodendrocytes, as well as a network of astrocytes and an associated vascular supply. A single oligodendrocyte can myelinate and interconnect as many as 60 segments on different axons. Myelinated segments are separated by the Nodes of Ranvier, and physical interactions between the oligodendrocyte and axon occur at paranodal junctions via anchorage of the axonal cytoskeleton to the oligodendrocyte through interactions of several adhesion molecules, including Caspr and contactin (on the axon-side) with neurofascin 155 (on the oligodendrocyte side) (Peles et al. 1997; Charles et al. 2002). This paranodal axo-glial junction has been described as 'by far the largest intracellular adhesion complex found in vertebrate biololgy' (Sherman and Brophy 2005). Astrocytes may also contribute to mechanical coupling via separate contacts with blood vessels in formation of the blood–brain barrier, and with axons at Nodes of Ranvier through the cell adhesion molecule Necl-1 (Butt et al. 1994; Kakunaga et al. 2005). Thus, glia physically interconnect other cellular and tissue entities to potentially act as a kind of 'cellular cross-link'. These interactions could alter the mechanical behavior of the individual axons by forcing composite behavior of axons, which demonstrate non-affine, uncoupled behavior at low stretch levels, but become increasingly coupled as stretch increases (Bain et al. 2003; Hao and Shreiber 2007). Thus, both astrocytes and oligodendrocytes (and the myelin oligodendrocytes produce) may contribute to the 'glue' that holds CNS tissue together.

In this study, we selectively interfered with the network of glia to examine how astrocytes and oligodendrocyte influence bulk mechanical characteristics of spinal cord tissue, which includes a significant white matter component. We chose two different but well-accepted methods to disrupt the glial matrix: chemically, by exposure to ethidium bromide (EB), which is cytotoxic to astrocytes and oligodendrocytes (Graca and Blakemore 1986; Reynolds et al. 1996); and immunologically, by exposing CNS myelin to an antibody targeted against galactocerebroside (GalC) along with serum complement, which disrupts myelination, and therefore oligodendrocyte-mediated connectivity of axons, without astrocyte loss (Keirstead et al. 1992, 1997). We found that both methods resulted in significant changes in the stress–strain response of spinal cord tissue in uniaxial tension, which suggests that both types of glia and myelin are important components of the structure–function relationship in spinal cord tissue.

## 2 Methods

### 2.1 Developmental myelin suppression

Fresh fertile chicken eggs (Charles River, Wilmington, MA, USA) were incubated at 38°C and 100% humidity. At the appropriate day (described below), a small window was created in the shell. One of four different reagents was injected with a microsyringe (Hamilton, Reno, NV, USA): 0.01% EB (Sigma, St. Louis, MO, USA) in 0.1% saline; 0.1% saline solution as a control for EB; an IgG rabbit-$\alpha$GalC antibody

(Chemicon International Inc., Temecula, CA, USA) at a dilution of 1:25 with 20% serum complement in 0.1 M PBS; or pure rabbit IgG (Jackson ImmunoResearch Laboratories, West Grove, PA, USA) at a 1:25 dilution with serum complement as a control for $\alpha$GalC. The $\alpha$GalC and IgG were injected in E12 spinal cords. EB and saline were injected into E14 spinal cords. Each embryo received two injections of 3 µl—one directly into the cervical spinal cord and one directly into the thoracic spinal cord. The window was covered with cellophane tape, and the eggs were returned to the incubator for further development. Separate, unoperated eggs served as additional controls. At E18, the spinal cords were excised for characterization.

### 2.2 Myelination visualization and quantification

Myelination was examined in two ways: myelin basic protein (MBP) immunohistochemistry and osmium tetroxide treatment. For immunohistochemical labeling, spinal cords from each treatment group were harvested at E18 and immersion fixed in 4% paraformaldehyde, followed by incubation in 20% sucrose-saline solution overnight at 4°C for cryoprotection. Frozen longitudinal sections were cut with a cryostat (ThermoShandon, Pittsburgh, PA, USA). Sections were double-labeled with a 1:400 dilution of rabbit anti-myelin basic protein (MBP) (Accurate Chemical Scientific, Westbury, NY, USA), and a 1:1,000 dilution of mouse $\alpha$-NF-200 (Sigma), followed by incubation in goat anti-rabbit Alexa 488 to visualize the MBP and goat anti-mouse Alexa 546 (Molecular Probes, Eugene, OR, USA) to visualize the neurofilaments. For osmium treatment, frozen transverse sections (5 µm) were placed on pre-treated glass microslides (Fisher Scientific, Hampton, NH, USA). Slides were treated in 2% osmium tetroxide (Electron Microscopy Sciences, Hatfield, PA, USA) for 30 min and dehydrated in a series of alcohol washes. Slides were cleared with xylene (Sigma), coverslipped, and the number of myelin sheaths was counted under brightfield microscopy at high magnification (Olympus IX81, Olympus Scientific, Westbury, NY, USA). Three spinal cords were examined for each experimental condition. Five sections were taken for each spinal cord, and five areas within the white matter were selected randomly from each section. The average number of myelin sheaths was determined for each slice, each spinal cord, and each condition and normalized to the control condition.

### 2.3 Astrocyte and oligodendrocyte immunoreactivity

The effects of injection of demyelinating agents or vehicles on glia were examined by immunohistochemically labeling cells for glial fibrillar acidic protein (GFAP) or GalC. Longitudinal sections (10 µm) were immunolabeled as above with a 1:100 dilution of mouse anti-GFAP (Sigma) or a 1:10 dilution of rabbit anti-GalC (Chemicon), followed by a 1:400 dilution of Alexa 488 goat anti-mouse secondary antibody.

### 2.4 Uniaxial tensile testing

The effects of glia on bulk tissue mechanics were evaluated by stretching spinal cords in uniaxial, low strain rate tension until failure. The full spinal column with spinal cord intact was excised from E18 chick embryos. The ventral surface of the spinal cord was exposed. The gauge length of a segment of the spinal cord beginning at the first nerve root after the cervical enlargement and extending rostrally for 11 segments was measured. Each measurement was repeated three times to obtain the average in situ length. The dorsal half of the vertebrae was removed, which allowed free retraction of the spinal cord, and the length of spinal cord was re-measured three times to obtain the average in vitro length. The spinal cord was visually checked with a dissection microscope (Zeiss, Westbury, NY, USA) for any abnormalities or damage that may have occurred during its removal. A 12 mm section of spinal cord was precisely marked off with two dots of reflective plastic (glitter). Three other dots were also placed along the spinal cord surface within the same 12 mm region to allow for assessment of strain uniformity during testing. Major and minor axes of the cord were also measured within the region with digital calipers. Measurements were taken upon initial contact with the tissue before any obvious compression occurred (Bylski et al. 1986) and the cross-sectional area of the spinal cord was calculated as an ellipse.

Uniaxial testing was performed using a Bose/Enduratec ELF 3200 (Electroforce Systems Group, Bose Corporation, Eden Prairie, MN, USA) with a 0.5 N cantilever load cell (Measurement Specialties, Hampton, VA, USA). The ends of the samples were placed on separate polyethylene plates that were attached 10 mm apart to either the load cell or crosshead. The glitter marking the ends of the 12 mm segment were placed exactly at the edges of plastic plates. The 2 mm slack ensured that the spinal cord was not stretched when originally placed in the testing device. The ends of the spinal cord were then fixed to the two plastic plates via a cyanoacrylate adhesive (Loctite Superglue, Henkel Consumer Adhesives, Inc., Avon, OH, USA). Hydration of the samples was maintained throughout the entire testing process with an ultrasonic mister (Wachsmuth & Krogmann, Elk Grove Village, IL, USA) placed directly beneath the sample. A schematic and an image of a spinal cord in the testing setup are shown in Fig. 1.

The spinal cords were stretched at 0.012 mm/s corresponding to an approximate $0.001\,s^{-1}$ strain rate. Due to the delicacy of the tissue, no preconditioning was applied (Georges et al. 2006). Each sample was tested only once and all tests were performed at room temperature. Load and displacement were recorded at 1.67 Hz. Load was converted

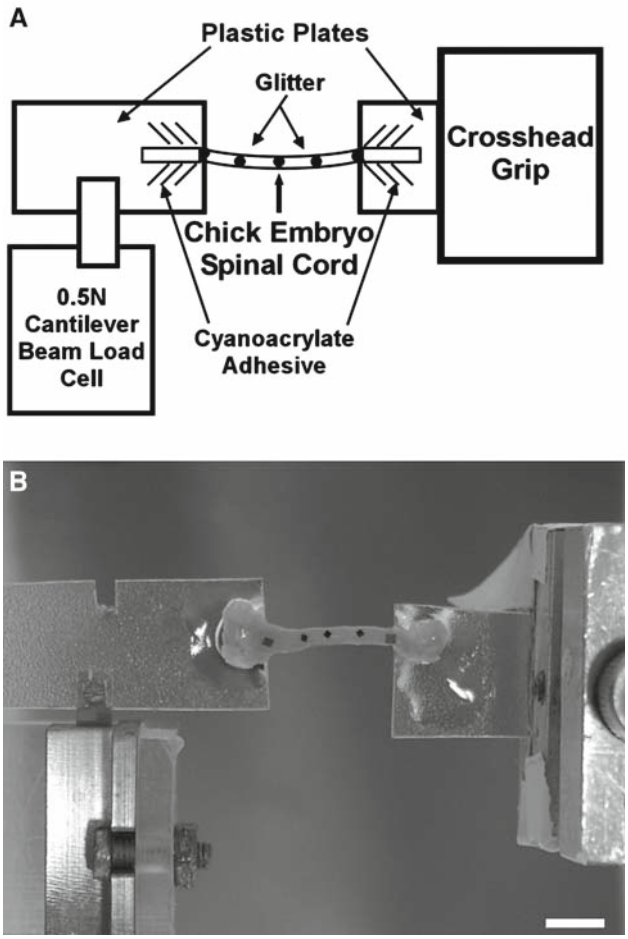


**Fig. 1** **a** Schematic of testing setup. The spinal cords were secured by gluing the ends of the sample to plastic plates attached to either the load cell or the actuator. Small pieces of reflective plastic (glitter) were used to track tissue displacement. **b** A sample in the setup. *Bar* 5 mm

to nominal stress by dividing by the cross-sectional area. The initial length was defined as the in situ length of the tested 12 mm segment of the spinal cord, which was determined from the percentage of shrinkage of the tissue upon full removal from the spinal column. Stress was plotted against stretch, and the ultimate tensile stress, $\sigma_{\mathrm{UTS}}$ and stretch at ultimate tensile stress, $\lambda_{\mathrm{UTS}}$ were identified as the highest stress achieved and the stretch at that stress, respectively. The stress–stretch data, which demonstrated non-linear, strain-stiffening behavior, was fit to a first-order Ogden strain energy potential function ($W$) assuming incompressible behavior, which has previously been used to describe behavior of the spinal cord (Bilston and Thibault 1996):

$$W = \frac{2G}{\alpha^2}\left(\lambda_1^{\alpha} + \lambda_2^{\alpha} + \lambda_3^{\alpha} - 3\right) \tag{1}$$

where $\lambda_i$ are the deviatoric principal stretches, $G$ represents the shear modulus, and $\alpha$ is a material-dependent parameter that introduces non-linear behavior. For uniaxial tension, the relationship between nominal stress and stretch ratio for a one-term Ogden material is

$$\sigma = \frac{2G}{\alpha}\left(\lambda_1^{\alpha-1} - \lambda_1^{-0.5\alpha-1}\right) \tag{2}$$

Kaleidagraph (Synergy Software, Reading, PA, USA) was used to identify the constants $G$ and $\alpha$ from the stress–stretch data.

### 2.5 Strain distribution analysis

To asses the uniformity of strain along the sample, images were taken every 0.5 mm (~40 s) with a digital camera (Samsung) secured to the top of the testing device. The length of each of the regions formed by the glitter was measured from the images (Microsuite analysis software, Olympus Scientific, Melville, NY, USA). For each segment, the stretch ratio was calculated and normalized to the overall stretch ratio of the spinal cord. Normalized values of 1 indicated a uniform distribution of strain along the length of the cord (Bain and Meaney 2000).

## 3 Results

### 3.1 Growth of chick embryo spinal cords

Although chick embryos uniformly survived the windowing and injection procedure, physical growth was affected by both EB and αGalC (Table 1). In spinal cords treated with EB or αGalC, significant decreases in length compared to controls (ANOVA, followed by pairwise comparisons with Fisher's Least Significant Difference (LSD) test, $P < 0.001$) were identified. No differences in saline or IgG controls ($P = 0.142$, $P = 0.404$, respectively) were detected compared to untreated controls. No differences were seen in the cross-sectional area for any condition (ANOVA, $P = 0.075$).

### 3.2 Myelination characterization

Spinal cords injected with saline or IgG showed similar MBP immunoreactivity to unoperated controls, with prominent immunolabeling in white matter, whereas spinal cords injected with either EB or αGalC showed a dramatic decrease in immunoreactivity spanning the spinal cord segment (Fig. 2), including the region tested mechanically. Significant differences in the number of myelinated axons were detected among all conditions (ANOVA, $P < 0.001$). Post hoc analysis demonstrated that myelination in saline-injected ($P = 0.530$) and IgG-injected ($P = 0.325$) spinal cords was not different than controls, but was significantly different following injection with either EB or αGalC than the appropriate

**Table 1** Length and area measurements of E18 spinal cords

| | EB ($n = 6$) | Saline ($n = 5$) | $\alpha$GalC ($n = 5$) | IgG ($n = 5$) | Control ($n = 6$) |
|---|---|---|---|---|---|
| Length (mm) | 22.35 ± 0.20* | 22.83 ± 0.25 | 21.99 ± 0.35* | 22.89 ± 0.36 | 23.02 ± 0.49 |
| Area ($mm^2$) | 1.47 ± 0.05 | 1.52 ± 0.04 | 1.48 ± 0.04 | 1.58 ± 0.11 | 1.51 ± 0.02 |

* Significantly different than controls, ANOVA followed by Fisher's LSD post hoc test for significance, $P < 0.05$

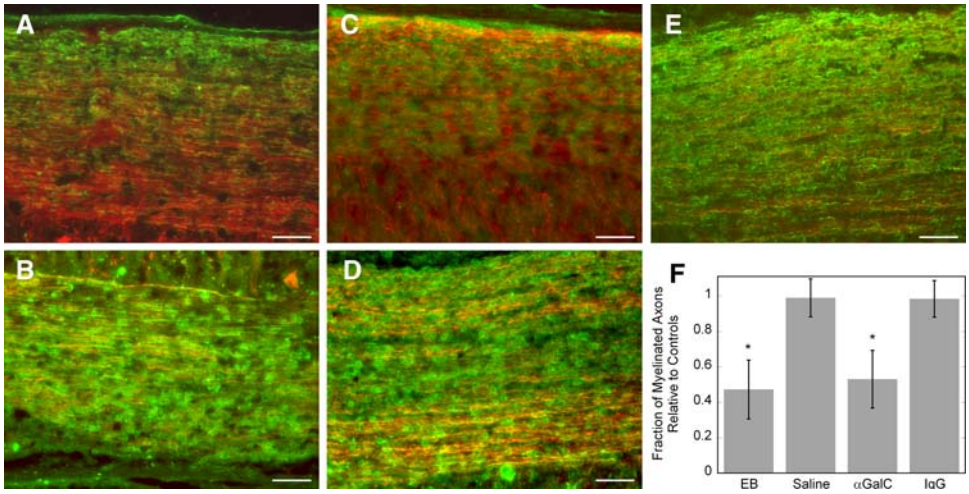


**Fig. 2** Demyelination following disruption of the glial matrix. $\alpha$-MBP immunofluorescence (*green*) was decreased following injection of EB (**a**) compared to saline (**b**), and injection of $\alpha$GalC with serum complement (**c**) compared to IgG with serum complement (**d**). Untreated control is shown in (**e**). Neurofilaments ($\alpha$-NF200) are shown in red. The average number (±SD) of myelinated fibers relative to unoperated controls was estimated in osmium-treated cross-sections (**f**). The number of fibers did not differ among comparisons of saline, IgG, and unoperated controls, but was significantly decreased following disruption of the glial matrix with either EB or $\alpha$GalC (ANOVA, followed by pairwise comparisons with Fisher's LSD test, $P < 0.001$). *Bar* 50 µm

control ($P < 0.001$). No overt differences were observed qualitatively in axons based on neurofilament labeling.

### 3.3 Glia characterization

The effects of the demyelinating protocols on glia were assessed qualitatively by immunohistochemically staining for astrocytes with $\alpha$-GFAP (Fig. 3) and oligodendrocytes with $\alpha$-GalC (Fig. 4). The GFAP and GalC immunoreactivity in spinal cords injected with saline, IgG, or $\alpha$GalC were very similar to unoperated controls, whereas EB injection clearly affected both astrocytes and oligodendrocytes. GFAP immunoreactivity revealed an interwoven network of cells with typical astrocyte morphology that was dramatically decreased only following treatment with EB. GalC immunoreactivity presented as focal punctate clusters consistent with previous reports (Fitzner et al. 2006), which was again reduced only in the EB-treated spinal cords.

### 3.4 Mechanical behavior

Chick embryo spinal cords displayed non-linear, strain-stiffening tensile stress–strain behavior indicative of weak fibrous composites. Representative plots for each condition are shown in Fig. 5. Small drops in stress followed by a recovery were commonly observed, and the frequency and magnitude of the drops generally increased with increasing stretch. Even after the ultimate tensile stretch was reached, small recoveries of stress were observed before complete failure. The behavior was consistent with microfailures and subsequent re-distribution of the remaining load, which is evident in plots of the tensile response of peripheral nerves (Borschel et al. 2003). Analysis of the strain distribution indicated that the stretch ratio of each segment varied within a spinal cord, but that this variation was not consistent among different samples, and was less than 2% from the ideal stretch ratio of one up until ~ 20–30% stretch.

Despite the inherent inconsistencies introduced by the microtears, the general behavior was consistent within an experimental condition, which enabled comparisons across conditions. Figure 6 displays portions of the stress–strain curves grouped according to different conditions. Significant overlap is apparent in the spread of data from control, saline-injected, and IgG-injected spinal cords. The EB- and $\alpha$GalC-demyelinated spinal cords demonstrate shallower stress– strain curves than their respective controls, but similar

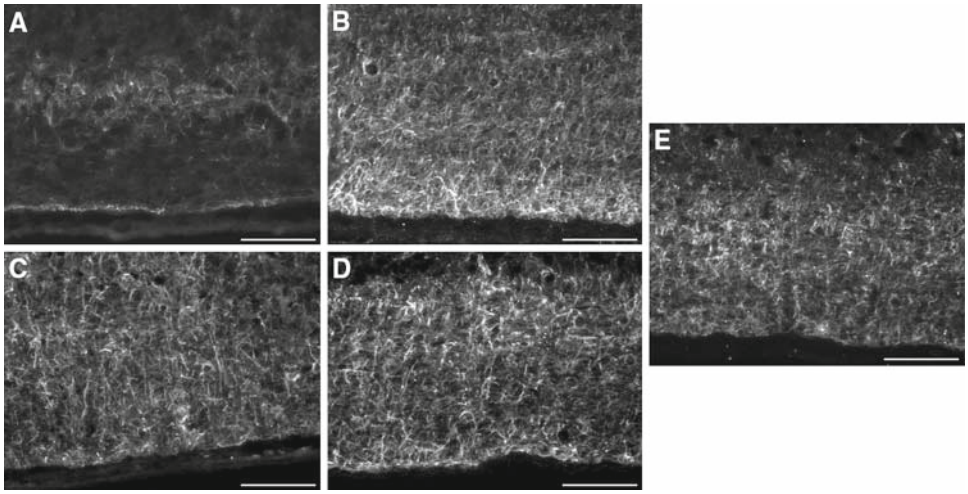


**Fig. 3** GFAP immunoreactivity following disruption of the glial matrix. Treatment with EB (**a**) produced an overt decrease in immunolabeling of astrocytes compared to saline-injected controls (**b**), whereas treatment with $\alpha$GalC (**c**) produced no obvious differences in GFAP labeling compared to IgG (**d**) or unoperated controls (**e**). *Bar* 50 μm

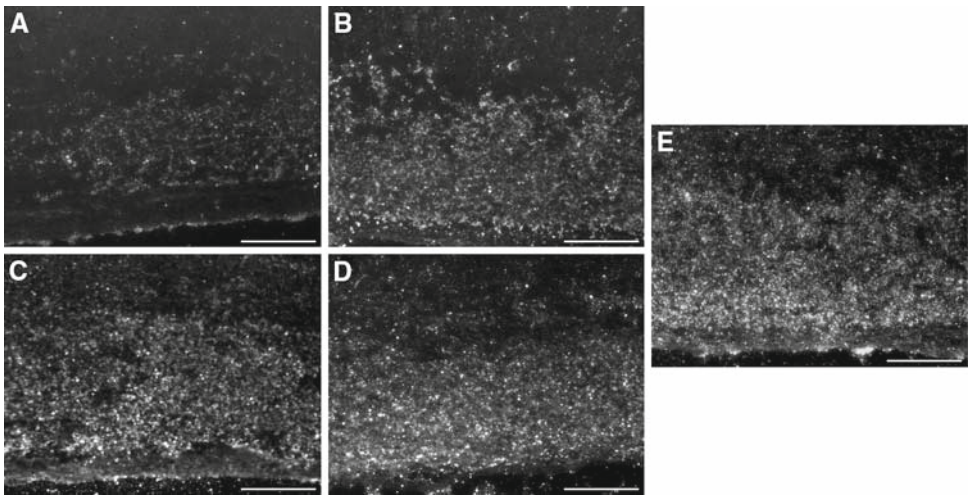


**Fig. 4** GalC immunoreactivity following disruption of the glial matrix. Treatment with EB (**a**) produced an overt decrease in immunolabeling of oligodendrocytes compared to saline-treated controls (**b**). The saline-treated, $\alpha$GalC-treated (**c**), and IgG-treated (**d**) spinal cords showed similar patterns of labeling to unoperated controls (**e**). *Bar* 50 μm

curves to each other. These observations are reflected in the 95th percentile confidence intervals for the average stress–strain data shown in Fig. 7.

To compare the stress–strain profiles quantitatively among the different conditions, the portions of individual curves up to 25% stretch were fit to an Ogden hyperelastic strain energy density function (Fig. 8). The strain-stiffening portions of the curve were well-represented by the Ogden model. All fits had $R^2$ correlation coefficients greater than 0.99. $\sigma_{\mathrm{UTS}}$ and $\lambda_{\mathrm{UTS}}$ were also identified from the stress–stretch curves (Table 2). The frequent drops in stress precluded the identification of a traditional yield stress, and we note that the results of the Ogden fit were viewed as measures of the relative stiffness of the tissue, rather than values for hyperelastic constitutive properties, to enable quantitative comparisons among conditions. Additionally, the Ogden model is for isotropic samples, and, though it has been used previously to describe the tensile properties of the spinal cord (Bilston and Thibault 1996), the fibrous nature of the white matter of the spinal cord likely induces anisotropy (Arbogast and Margulies 1999). As such, the results of the fit are representative of the axial response to tensile loading only. ANOVA detected significant differences in $\sigma_{\mathrm{UTS}}$ ($P = 0.002$) and in $G$ ($P = 0.006$) among all conditions. Post hoc pairwise comparisons identified no significant difference between operated and unoperated control conditions for either measure (min $P = 0.622$ for $\sigma_{\mathrm{UTS}}$ and min $P = 0.449$ for $G$). Post hoc pairwise comparisons demonstrated that the $\sigma_{\mathrm{UTS}}$ of EB-injected ($P = 0.004$) and $\alpha$GalC-injected ($P = 0.023$) spinal cords were significantly less than their respective controls, but not different than each other ($P = 0.087$). Similarly, significant differences were identified in $G$ between EB and saline ($P = 0.022$), and $\alpha$GalC and IgG ($P = 0.018$), but no differences were found when the two treatments were compared to each other ($P = 0.993$). Although $\lambda_{\mathrm{UTS}}$ decreased in EB-injected tissues compared to the other conditions, no significant differences were observed following initial comparison with ANOVA ($P = 0.708$). No significant differences were observed for the value of $\alpha$ (ANOVA, $P = 0.950$).

**Table 2** Summary of mechanical testing results

| | EB | Saline | αGalC | IgG | Control |
|---|---|---|---|---|---|
| $\sigma_{UTS}$(kPa) | 28.4 ± 9.38* | 77.8 ± 19.6 | 55.9 ± 28.9* | 93.5 +/ 37.3 | 85.2 ± 17.7 |
| $\lambda_{UTS}$ | 1.38 ± 0.09 | 1.43 ± 0.09 | 1.45 ± 0.10 | 1.45 ± 0.10 | 1.42 ± 0.03 |
| $G$(kPa) | 17.4 ± 5.70* | 29.2 ± 7.38 | 17.7 ± 6.80* | 30.0 ± 7.26 | 32.8 ± 9.53 |
| $\alpha$ | 8.32 ± 2.55 | 8.49 ± 1.34 | 8.74 ± 0.84 | 9.00 ± 1.62 | 8.22 ± 1.27 |

* Significantly different than controls, ANOVA, followed by post hoc pairwise comparisons with Fisher's LSD, $P < 0.05$

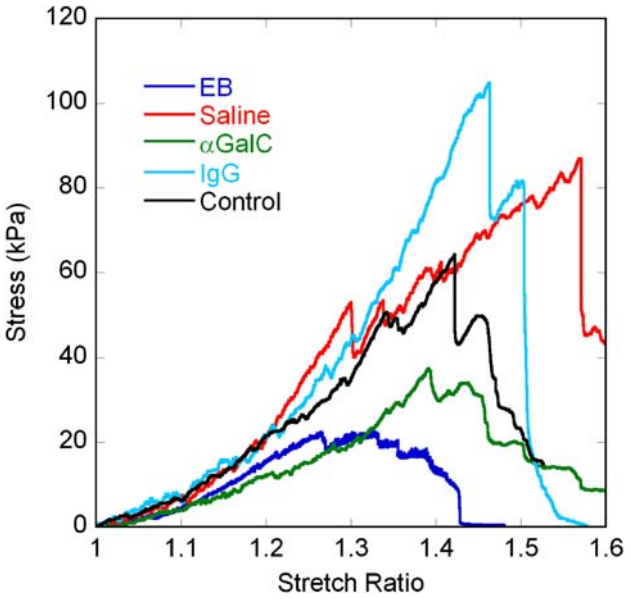


**Fig. 5** Representative tensile stress–stretch curves for the different conditions. Although the response was generally non-linear, for each condition, sharp fluctuations in stress were observed, which is indicative of microfailures in the tissue

## 4 Discussion

Despite the historical classification of glia as the glue of the brain and spinal cord and/or the structural scaffold for these tissues, little has been done to characterize this role. Recent evidence identifying the mechanical characteristics of glia and neurons (Lu et al. 2006), documenting distinct regional mechanical and kinematic properties in the developing brain and spinal cord (Elkin et al. 2007; Hao and Shreiber 2007), and demonstrating differences in the phenotypic response of astroglia and neurons to substrates with different compliance (Flanagan et al. 2002; Georges et al. 2006), prompted us to examine more specifically the role of the glial matrix in providing mechanical support to the spinal cord. We found substantial decreases in the tensile mechanical properties of the chick embryo spinal cord following partial disruption of the glial matrix, indicating that the glial matrix, including astroglia, oligodendroglia, and myelin, does indeed provide significant structural support to the tissue.

Both EB and αGalC treatments produced significant changes in the tensile behavior of the spinal cord, and they likely share some common affects on tissue structure and introduce important differences. Both techniques are well-accepted and commonly used to demyelinate tissue, primarily in models of multiple sclerosis (MS) as well as to evaluate the natural time course of and therapeutic approaches for remyelination (Graca and Blakemore 1986; Fernandes et al. 1998; Pereira et al. 1998). EB is a DNA-intercalating dye that is cytotoxic to dividing cells, which disrupts the glial matrix by selectively killing astrocytes and oligodendrocytes, and can also disrupt the blood–brain barrier, while preserving neurons (Fernandes et al. 1998; Pereira et al. 1998). While no reports of the use of EB in chick embryo models were found, our results were consistent with those found in other species, where demyelination is observed with a few days of injection. Structurally, in addition to demyelinating, EB-mediated disruption would decrease cellularity and interfere with inter- and intraconnectivity among axons and the vasculature via damage to oligodendroglia and astrocytes.

Ethidium bromide also potentially damages cells responsible for maintenance of other connective tissue that may influence the mechanical properties. It has been reported that the stiffness of freshly excised peripheral nerve did not change following acellularization with detergent baths, which removed all axons, Schwann cells, and myelin and left a lattice of extracellular matrix, though some of the failure properties did decrease (Borschel et al. 2003). When compared to peripheral nerves, the spinal cord has minimal structural extracellular matrix. Nevertheless, we attempted to estimate the contribution of connective tissue to the properties of the fully decellularized spinal cord by testing control E18 explants treated with the protocol described in Borschel et al (Borschel et al. 2003). The decellularized spinal cords provided little resistance to tension and did not produce enough load to register with our force transducer during uniaxial testing (data not shown).

Unlike EB, αGalC causes demyelination without damage to astrocytes or axons (Carroll et al. 1987; Dyer and Benjamins 1990). Galactocerebroside is a major sphingolipid constituent of myelin (Sergott et al. 1984; Mastaglia et al. 1989). The αGalC treatment is one of several options to study MS via induction of experimental allergic encephalomyelitis,

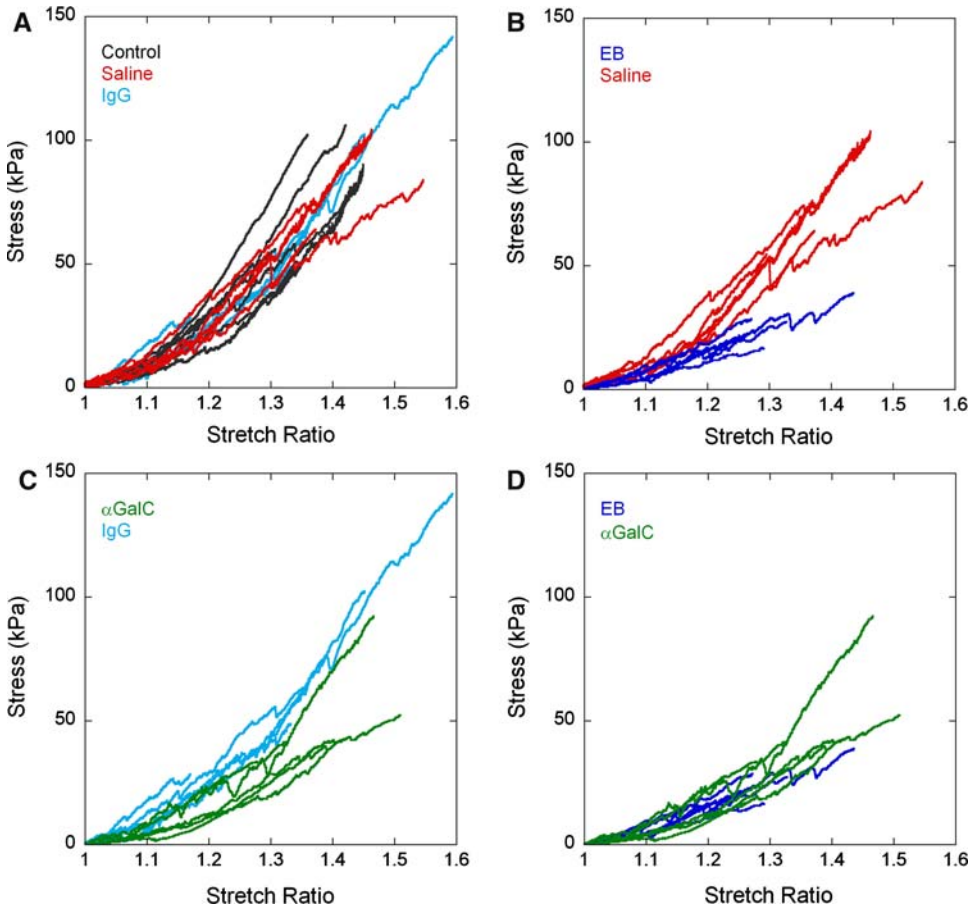


**Fig. 6** Stress–stretch data in the strain-stiffening regime demonstrating spread for each condition. Despite the influence of the microfailures, the stress–stretch response was consistent among untreated, saline-injected, and IgG-injected control conditions (**a**). Demyelinating with EB (**b**) or with $\alpha$GalC (**c**) consistently decreased the stiffness of the tissue compared to their respective controls. The two demyelinating protocols resulted in similar stress–stretch data (**d**)

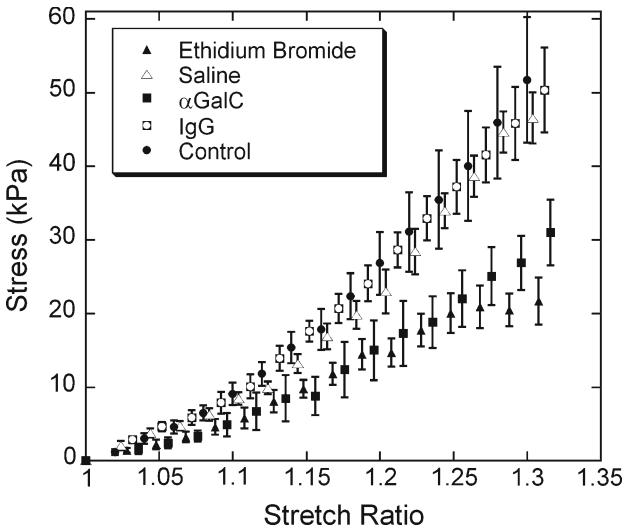


**Fig. 7** Average stress–stretch response of the chick embryo spinal cord in the strain-stiffening regime. Significant overlap of the 95% confidence intervals was observed for the saline (*open triangles*), IgG (*open squares*), and untreated controls (*closed circles*); separate overlap was observed for the EB (*closed triangles*) and $\alpha$GalC (*closed squares*) treated spinal cords, but the slopes were lower than the controls

and antibodies against galactocerebroside are often used as a clinical marker of MS. The effects of the treatment on oligodendrocytes and the mechanism of demyelination remain debated. In vitro, exposure to $\alpha$GalC + complement has been reported to be cytotoxic to rat and bovine oligodendrocytes in dose- and duration-dependent manners, which suggests that oligodendrocytes may be selectively vulnerable. However, others have shown that $\alpha$GalC can cause demyelination without damage to astrocytes or axons, and potentially without damage to oligodendrocytes (Ozawa et al. 1989; Keirstead et al. 1992). Specifically, injection of $\alpha$GalC plus complement into the developing chick spinal cord prior to myelination (E9–E12) has been shown to delay the onset of myelination without significant cell death or altered neuronal development (Keirstead et al. 1992), and our results were consistent with these reports.

Together, these results indicate that demyelination along with partial acellularization of the spinal cord with EB, and with minimal acellularization but disruption of axonal connectivity via $\alpha$GalC significantly decreases stiffness and failure properties. This suggests that, in addition to biological functions, myelin and glia also may provide protection

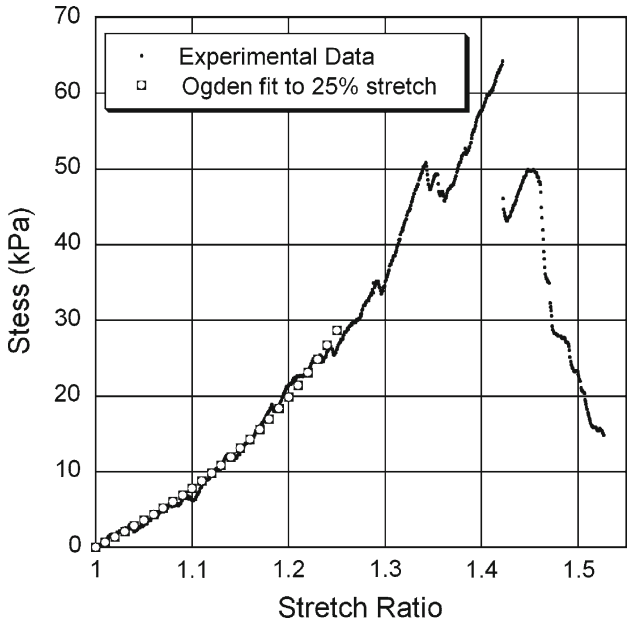


**Fig. 8** Representative fit of Ogden model to stress–stretch data. Stress–stretch data from each experiment was fit with the Ogden strain energy density function up to 25% stretch to identify the parameters $G$ and $\alpha$, which characterize generally the stiffness and non-linearity of the tissue. These parameters are compared among conditions in Table 2

against excessive tensile stresses and strains to limit injury. The complex interconnectivity of astrocytes and oligodendrocytes with the vascular system and axonal network can serve to distribute stretch among the tissue's structural constituents and induce composite behavior. Since the prime mechanostructural components are living cells, rather than extracellular matrix, protection from mechanical loading via skeletal components becomes even more critical.

Importantly, we believe that it is not necessarily the myelin alone which couples the axons and/or bears the brunt of the physical resistance; rather, myelination may serve as documentation of the interconnectivity of axons via oligodendrocytes. Previous reports have produced conflicting results regarding the influence of glia on mechanical properties. Gefen et al. (2005) reported a decrease in the compressive properties of rat brain with development from post natal day 13 to 90, and argued that the increase in myelin and simultaneous decrease in water content led to the decrease in stiffness. A composite, continuum model of shear deformation of white matter in the brainstem, comprising viscoelastic 'fibers' representing axons embedded in a viscoelastic 'matrix' representing glia, predicted that the glial matrix was much more compliant than the axon fibers, and that increasing the volume fraction of matrix decreased the stiffness (Arbogast and Margulies 1999). A recent report by Lu et al. (2006) tested the properties of individual neurons and astrocytes with scanning force microscopy, and found neurons to be significantly stiffer than the glia.

Although differences in the mechanical properties of compact and non-compact myelin have been suggested based on AFM data from fixed peripheral nerves (Heredia et al. 2007) and from myelin extracted from bovine white matter (Mueller et al. 1999), no difference in myelinated axon properties was noted between unmyelinated nodes of Ranvier and myelinated internode segments, nor were significant differences detected between individual myelinated and demyelinated axons, which were harvested from wild type and transgenic, 'trembler' mice, respectively (Heredia et al. 2007). Thus, myelin in and of itself may not increase the stiffness of white matter. However, in addition to the significant cytoskeletal contact at axo-glial paranodal junctions, elevated adhesion occurs between apposing extraceullar membranes of an oligodendroglial myelinating process that is wrapped concentrically around an axon, forming a so-called glycosynapse, and perhaps causing adhesion between separate oligodendrocytes to additionally 'glue' the oligodendrocytes together. Both the myelin–myelin interactions and, especially, the paranodal axo-glial adhesions would place the Nodes of Ranvier at risk for deformation from a stress concentration, and elongation of the Nodes of Ranvier has been observed following non-disruptive stretch injury of the guinea pig optic nerve (Gennarelli et al. 1993).

An important distinction in our experiments versus previous characterizations could be the application of tension as the primary mode of deformation, versus compression or shear. Like any fiber, a single axon will behave differently in tension than in other deformation modes, and the myelin may directly affect its tensile properties and/or add to the parallel structures oriented in the direction of stretch. Moreover, in tension, a complex recruitment of axonal fibers and uncoiling of axons and other cellular processes occurs, which leads to a change in individual axon kinematics from uncoupled, non-affine behavior at low stretch levels to coupled, affine behavior at higher ones to alter the bulk mechanics of white matter (Bain et al. 2003). It was hypothesized that coupling to the glial matrix is responsible for the altered kinematics, which forces composite behavior and stiffens and strengthens the white matter (Meaney et al. 2003). We recently demonstrated that the transition to affine mechanics becomes progressively more significant with development during a period of rapid myelination in the chick embryo spinal cord (Hao and Shreiber 2007), although the observed changes could not be directly attributed to changes in the glial matrix because of the concomitant addition of axon tracts in the white matter and changes in connective tissue and vasculature.

While individual glia may be more compliant than their nearby neuronal or axonal neighbors, they significantly contribute to the overall stiffness and strength potentially by allowing many to act in unison and share the load. This role would be less significant in compressive and shear modes, where the tensile strains derived from deviatoric deformation

are substantially lower, and in these types of deformation, the soft, compliant nature of the glia may indeed provide a deformable buffer between neurons and meninges/bone, as suggested by Lu et al. (2006). However, since tension has been long regarded as the mode of injury for axons (Meaney et al. 2001), identifying the role of glia in this mode of deformation becomes more important for studies of traumatic brain and spinal cord injury.

The tensile experiments were performed on whole chick embryo spinal cord explants, including the meningeal layers, and comparison of saline- and IgG-injected cords to untreated controls demonstrates that piercing the dura, arachnoid, and pia mater did not alter the properties. Combined with the immunohistochemical data and myelination quantification, these results indicate that the injection procedure, and any subsequent inflammation, glial reactivity, and/or immune response, did not significantly affect the tissue, and that the observed changes in the mechanical response are due to the specific treatments. It is possible that myelin breakdown or cellular fragments following EB or $\alpha$GalC treatment triggered cellular responses from inflammatory cells and/or glia that contributed to the observed changes in mechanical properties. However, we believe that the changes in tissue mechanics indicate that the changes in tissue structure are responsible.

We selected the developing chick embryo spinal cord as our model tissue, which conferred several advantages for this study. Chick embryo tissue is readily available through procurement of fresh, fertilized eggs and is extremely cost effective when compared to small mammals. Maintaining eggs during development is relatively simple, as is harvesting tissue at a desired developmental stage. Additionally, it is possible to prevent or delay the onset of myelination (with $\alpha$GalC, for instance), rather than having to disrupt existing myelination, as would be necessary in a fully developed animal model. However, because the chick is developing rapidly, the treatments may cause changes in other tissue features that could affect the tensile response, and a comparison to adult tissue for application to injury mechanics is warranted. For example, transgenic mouse or rat models that involve dysmyelination via a variety of mutations may provide intriguing systems to further explore white matter mechanics. With regards to developmental mechanics, the process of myelination occurs over a period of weeks in the chick but in humans continues significantly after birth, and would alter the micro- and macro-scale stiffness of the tissue. As discussed by Lu et al. (Lu et al. 2006), neural cells may use the distinct mechanical properties presented by different cellular constituents as a cue for enhanced and/or directed growth or branching, as has been observed in vitro (Balgude et al. 2001; Flanagan et al. 2002; Georges et al. 2006), or potentially for differentiation (Discher et al. 2005), and the spatio-temporal distribution of cells becomes a map for subsequent growth and development.

**Acknowledgments** Funding for this research was provided by the Whitaker Foundation (RG 02-128).

## References

Arbogast KB, Margulies SS (1999) A fiber-reinforced composite model of the viscoelastic behavior of the brainstem in shear. J Biomech 32(8):865–870. doi:10.1016/S0021-9290(99)00042-1

Bain AC, Meaney DF (2000) Tissue-level thresholds for axonal damage in an experimental model of central nervous system white matter injury. J Biomech Eng 122(6):615–622. doi:10.1115/1.1324667

Bain AC, Shreiber DI, Meaney DF (2003) Modeling of microstructural kinematics during simple elongation of central nervous system tissue. J Biomech Eng 125(6):798–804. doi:10.1115/1.1632627

Balgude AP, Yu X, Szymanski A, Bellamkonda RV (2001) Agarose gel stiffness determines rate of DRG neurite extension in 3D cultures. Biomaterials 22(10):1077–1084. doi:10.1016/S0142-9612(00)00350-1

Bilston LE, Thibault LE (1996) The mechanical properties of the human cervical spinal cord in vitro. Ann Biomed Eng 24(1):67–74. doi:10.1007/BF02770996

Borschel GH, Kia KF, Kuzon WM Jr, Dennis RG (2003) Mechanical properties of acellular peripheral nerve. J Surg Res 114(2):133–139. doi:10.1016/S0022-4804(03)00255-5

Butt AM, Colquhoun K, Tutton M, Berry M (1994) Three-dimensional morphology of astrocytes and oligodendrocytes in the intact mouse optic nerve. J Neurocytol 23(8):469–485. doi:10.1007/BF01184071

Bylski DI, Kriewall TJ, Akkas N, Melvin JW (1986) Mechanical behavior of fetal dura mater under large deformation biaxial tension. J Biomech 19(1):19–26. doi:10.1016/0021-9290(86)90105-3

Carroll WM, Jennings AR, Mastaglia FL (1987) Reactive glial cells in CNS demyelination contain both GC and GFAP. Brain Res 411(2):364–369. doi:10.1016/0006-8993(87)91088-2

Charles P, Tait S, Faivre-Sarrailh C, Barbin G, Gunn-Moore F, Denisenko-Nehrbass N, et al (2002) Neurofascin is a glial receptor for the paranodin/Caspr-contactin axonal complex at the axoglial junction. Curr Biol 12(3):217–220. doi:10.1016/S0960-9822(01)00680-7

Discher DE, Janmey P, Wang YL (2005) Tissue cells feel and respond to the stiffness of their substrate. Science 310(5751):1139–1143. doi:10.1126/science.1116995

Dyer CA, Benjamins JA (1990) Glycolipids and transmembrane signaling: antibodies to galactocerebroside cause an influx of calcium in oligodendrocytes. J Cell Biol 111(2):625–633. doi:10.1083/jcb.111.2.625

Elkin BS, Azeloglu EU, Costa KD, Morrison B III (2007) Mechanical heterogeneity of the rat hippocampus measured by atomic force microscope indentation. J Neurotrauma 24(5):812–822. doi:10.1089/neu.2006.0169

Fernandes CG, Graca DL, Pereira LA (1998) Inflammatory response of the spinal cord to multiple episodes of blood–brain barrier disruption and toxic demyelination in Wistar rats. Braz J Med Biol Res 31(7):933–936. doi:10.1590/S0100-879X1998000700008

Fitzner D, Schneider A, Kippert A, Mobius W, Willig KI, Hell SW, et al (2006) Myelin basic protein-dependent plasma membrane reorganization in the formation of myelin. EMBO J 25(21):5037–5048. doi:10.1038/sj.emboj.7601376

Flanagan LA, Ju YE, Marg B, Osterfield M, Janmey PA (2002) Neurite branching on deformable substrates. Neuroreport 13(18):2411–2415. doi:10.1097/00001756-200212200-00007

Gefen A, Gefen N, Linder-Ganz E, Margulies SS (2005) In vivo muscle stiffening under bone compression promotes deep pressure sores. J Biomech Eng 127(3):512–524. doi:10.1115/1.1894386

Gennarelli TA, Tipperman R, Maxwell WL, Graham DI, Adams JH, Irvine A (1993) Traumatic damage to the nodal axolemma: an early, secondary injury. Acta Neurochir Suppl (Wien) 57:49–52

Georges PC, Miller WJ, Meaney DF, Sawyer ES, Janmey PA (2006) Matrices with compliance comparable to that of brain tissue select neuronal over glial growth in mixed cortical cultures. Biophys J 90(8):3012–3018. doi:10.1529/biophysj.105.073114

Graca DL, Blakemore WF (1986) Delayed remyelination in rat spinal cord following ethidium bromide injection. Neuropathol Appl Neurobiol 12(6):593–605. doi:10.1111/j.1365-2990.1986.tb00162.x

Hao H, Shreiber DI (2007) Axon kinematics change during growth and development. J Biomech Eng 129(4):511. doi:10.1115/1.2746372

Heidemann SR, Buxbaum RE (1994) Mechanical tension as a regulator of axonal development. Neurotoxicology 15(1):95–107

Heredia A, Bui CC, Suter U, Young P, Schaffer TE (2007) AFM combines functional and morphological analysis of peripheral myelinated and demyelinated nerve fibers. Neuroimage 37(4):1218–1226. doi:10.1016/j.neuroimage.2007.06.007

Kakunaga S, Ikeda W, Itoh S, Deguchi-Tawarada M, Ohtsuka T, Mizoguchi A, et al (2005) Nectin-like molecule-1/TSLL1/SynCAM3: a neural tissue-specific immunoglobulin-like cell-cell adhesion molecule localizing at non-junctional contact sites of presynaptic nerve terminals, axons and glia cell processes. J Cell Sci 118(Pt 6):1267–1277. doi:10.1242/jcs.01656

Keirstead HS, Hasan SJ, Muir GD, Steeves JD (1992) Suppression of the onset of myelination extends the permissive period for the functional repair of embryonic spinal cord. Proc Natl Acad Sci USA 89(24):11664–11668. doi:10.1073/pnas.89.24.11664

Keirstead HS, Pataky DM, McGraw J, Steeves JD (1997) In vivo immunological suppression of spinal cord myelin development. Brain Res Bull 44(6):727–734. doi:10.1016/S0361-9230(97)00374-2

Lu YB, Franze K, Seifert G, Steinhauser C, Kirchhoff F, Wolburg H, et al (2006) Viscoelastic properties of individual glial cells and neurons in the CNS. Proc Natl Acad Sci USA 103(47):17759–17764. doi:10.1073/pnas.0606150103

Mastaglia FL, Carroll WM, Jennings AR (1989) Spinal cord lesions induced by antigalactocerebroside serum. Clin Exp Neurol 26:33–44

Meaney DF (2003) Relationship between structural modeling and hyperelastic material behavior: application to CNS white matter. Biomech Model Mechanobiol 1(4):279–293. doi:10.1007/s10237-002-0020-1

Meaney DF, Margulies SS, Smith DH (2001) Diffuse axonal injury. J Neurosurg 95(6):1108–1110

Mueller H, Butt HJ, Bamberg E (1999) Force measurements on myelin basic protein adsorbed to mica and lipid bilayer surfaces done with the atomic force microscope. Biophys J 76(2):1072–1079

Ozawa K, Saida T, Saida K, Nishitani H, Kameyama M (1989) In vivo CNS demyelination mediated by anti-galactocerebroside antibody. Acta Neuropathol 77(6):621–628. doi:10.1007/BF00687890

Peles E, Nativ M, Lustig M, Grumet M, Schilling J, Martinez R, et al (1997) Identification of a novel contactin-associated transmembrane receptor with multiple domains implicated in protein-protein interactions. EMBO J 16(5):978–988. doi:10.1093/emboj/16.5.978

Pereira LA, Dertkigil MS, Graca DL, Cruz-Hofling MA (1998) Dynamics of remyelination in the brain of adult rats after exposure to ethidium bromide. J Submicrosc Cytol Pathol 30(3):341–348

Reynolds R, di Bello IC, Meeson A, Piddlesden S (1996) Comparison of a Chemically Mediated and an Immunologically Mediated Demyelinating Lesion Model. Methods 10(3):440–452. doi:10.1006/meth.1996.0122

Schultze M (1866).Zur Anatomie und Physiologe der Retina. Max Cohen & Sons, Bonn

Sergott RC, Brown MJ, Silberberg DH, Lisak RP (1984) Antigalactocerebroside serum demyelinates optic nerve in vivo. J Neurol Sci 64(3):297–303. doi:10.1016/0022-510X(84)90177-1

Sherman DL, Brophy PJ (2005) Mechanisms of axon ensheathment and myelin growth. Nat Rev Neurosci 6(9):683–690. doi:10.1038/nrn1743

Virchow (1856).Gesammelte Abhandlungen zur Wissenschafilichen medicin. Meidinger Sohn, Frankfurt

Volterra A, Meldolesi J (2005) Astrocytes, from brain glue to communication elements: the revolution continues. Nat Rev Neurosci 6(8):626–640. doi:10.1038/nrn1722

Yuan Q, Dougherty L, Margulies SS (1998) In vivo human cervical spinal cord deformation and displacement in flexion. Spine 23(15):1677–1683. doi:10.1097/00007632-199808010-00012